

RESEARCH ARTICLE

Quantitative SPECT/CT Imaging of ^{177}Lu with *In Vivo* Validation in Patients Undergoing Peptide Receptor Radionuclide Therapy

J. C. Sanders,^{1,2} T. Kuwert,² J. Hornegger,¹ P. Ritt^{1,2}

¹Pattern Recognition Lab, Department of Computer Science, University of Erlangen-Nuremberg, Martensstr. 3, 91058, Erlangen, Germany

²Clinic of Nuclear Medicine, University Hospital Erlangen, University of Erlangen-Nuremberg, Ulmenweg 18, 91054, Erlangen, Germany

Abstract

Purpose: The purpose of this study is to extend an established SPECT/CT quantitation protocol to ^{177}Lu and validate it *in vivo* using urine samples, thus providing a basis for 3D dosimetry of ^{177}Lu radiotherapy and improvement over current planar methods which improperly account for anatomical variations, attenuation, and overlapping organs.

Procedures: In our quantitation protocol, counts in images reconstructed using an ordered subset-expectation maximization algorithm are converted to kilobecquerels per milliliter using a calibration factor derived from a phantom experiment. While varying reconstruction parameters, we tracked the ratio of image to true activity concentration (recovery coefficient, RC) in hot spheres and a noise measure in a homogeneous region. The optimal parameter set was selected as the point where recovery in the largest three spheres (16, 8, and 4 ml) stagnated, while the noise continued to increase. Urine samples were collected following 12 SPECT/CT acquisitions of patients undergoing [^{177}Lu]DOTATATE therapy, and activity concentrations were measured in a well counter. Data was reconstructed using parameters chosen in the phantom experiment, and estimated activity concentration from the images was compared to the urine values to derive RCs.

Results: In phantom data, our chosen parameter set yielded RCs in 16, 8, and 4 ml spheres of 80.0, 74.1, and 64.5 %, respectively. For patients, the mean bladder RC was 96.1 ± 13.2 % (range, 80.6–122.4 %), with a 95 % confidence interval between 88.6 and 103.6 %. The mean error of SPECT/CT concentrations was 10.1 ± 8.3 % (range, –19.4–22.4 %).

Conclusions: Our results show that quantitative ^{177}Lu SPECT/CT *in vivo* is feasible but could benefit from improved reconstruction methods. Quantifying bladder activity is analogous to determining the amount of activity in the kidneys, an important task in dosimetry, and our results provide a useful benchmark for future efforts.

Key words: Quantitative SPECT, [^{177}Lu]DOTATATE, Peptide receptor radionuclide therapy, Dosimetry

Introduction

In recent years, Lutetium-177 has gained popularity for therapy applications due to the concentrated energy deposition of its low-energy beta emissions, a favorable

half-life, and its gamma emissions, which enable imaging. The range of applications includes ^{177}Lu labeled antibody treatments of renal cell carcinoma [1] and metastatic prostate cancer [2], as well as radiation synovectomy [3]. In addition to these relatively recent developments, a further, more established use of ^{177}Lu is the treatment of gastroenteropancreatic neuroendocrine tumors (GEP-NETs) by means of peptide receptor radionuclide therapy (PRRT).

Correspondence to: J. C. Sanders; e-mail: James.Sanders@uk-erlangen.de

PRRT exploits the characteristic overexpression of somatostatin receptors observed in NETs by mating a peptide with an affinity for them to a radioisotope. Early approaches based on high doses of ^{111}In -octreotide [4] were eventually replaced by ^{90}Y bound to various DOTA-chelated compounds such as DOTATOC [5], which offered longer overall survival times [6]. A comprehensive review of various PRRT options can be found in [7] and [8]. (^{177}Lu DOTA⁰,Tyr3)-octreotate (^{177}Lu DOTATATE) PRRT has been shown to have a higher tumor uptake and superior tumor-to-kidney ratio than [^{111}In]octreotide and [^{90}Y]DOTATOC [9, 10], and patients treated with [^{177}Lu]DOTATATE may experience fewer negative side effects associated with deterministic radiation effects while exhibiting superior tumor responses relative to [^{90}Y]DOTATOC and various chemotherapy treatments [11]. A significantly improved quality of life for patients undergoing therapy has also been noted [12].

The process of [^{177}Lu]DOTATATE PRRT begins with dosimetry, where the patient typically receives an injection of [^{111}In]octreotide with roughly similar binding properties to the therapy agent, followed by planar scintigraphy scans at various time points using a gamma camera. From these scans, dose to organs is estimated according to established procedures, such as Medical Internal Radiation Dose (MIRD) guidelines, and the appropriate therapy dose is determined [13]. This approach, however, is based on approximations about average organ geometry and not individualized for each patient. It is error prone due to an inability to properly handle cases where organs and/or tumors overlap each other and its reliance on data from a radiotracer such as [^{111}In]octreotide or -octreotate having different biokinetics from the therapy agent itself [4, 14]. An overestimation of dose may lead to undertreatment and lower chance of tumor response. Conversely, underestimation may result in side effects such as kidney damage.

Quantitative single photon emission-computed tomography imaging with an accompanying x-ray computed tomography scan for attenuation correction (SPECT/CT) can mitigate the geometric drawbacks mentioned above by offering three-dimensional representations of uptake patterns [15–17]. The problem of differences in radiopharmacology can be solved by imaging [^{177}Lu]DOTATATE directly, taking advantage of the gamma rays in its emission spectrum. An approach to direct dosimetry of [^{177}Lu]DOTATATE using SPECT/CT has been developed by Sandström et al. [18] and compared to the MIRD planar method. Results indicated that, particularly in patients with a large tumor burden and/or overlapping organs, the MIRD planar approach might be insufficient for proper dosimetry. A critical component of a SPECT/CT dosimetry method is the quantitative accuracy of the reconstructed images. The goal of this work was to further efforts towards SPECT/CT dosimetry for ^{177}Lu by extending an existing quantitative SPECT/CT procedure developed for $^{99\text{m}}\text{Tc}$ and to assess its accuracy *in vivo* using patient data.

Practices and Methods

Phantom Acquisition and Reconstruction

We performed two phantom acquisitions. For the first, we filled a homogeneous 6.2-l cylinder phantom with 307.5 MBq of ^{177}Lu to yield a concentration of 48.4 kBq/ml at the time of acquisition. For the second phantom acquisition, we prepared a dilution containing 19.0 MBq of ^{177}Lu mixed with 50 ml of water measured using a 25-ml graduated cylinder with a reported accuracy of ± 0.166 ml. This was used to fill a set of six spheres with volumes 16, 8, 4, 2, 1, and 0.5 ml which were attached to one end of a separate 6.1-l cylinder. The remaining background volume (6.03 l) contained 292 MBq, yielding sphere and background concentrations of 374.3 and 48.4 kBq/ml, respectively. Figure 1 shows a transaxial slice of the sphere phantom through these objects.

The acquisitions were performed on a Symbia TruePoint T2 SPECT/CT system (Siemens Molecular Imaging, Hoffman Estates) equipped with two gamma detector heads (9.5 mm crystal thickness) and a two-slice CT for attenuation correction. A total of 120 SPECT projections were acquired using Medium Energy Low Penetration (MELP) collimators (see Table 1).

Data was acquired in six energy windows: one from each of ^{177}Lu photopeaks (PP) using 20 % energy windows centered at 113 and 208 keV (PP₁₁₃ and PP₂₀₈, respectively), as well as from Upper and Lower Scatter (US and LS) windows immediately adjacent to each peak (US₁₁₃, US₂₀₈, LS₁₁₃, and LS₂₀₈). The scatter windows corresponding to the lower photopeak received widths of 15 % of the photopeak energy, and those of the upper peak were set to 20 %. This was done to avoid overlapping US₁₁₃ and LS₂₀₈ while keeping the scatter window pairs symmetric about their respective peaks. Following the SPECT, a CT was acquired for attenuation correction (AC). It should be noted that our scatter windows are wider than those originally proposed in [19]. However, this width

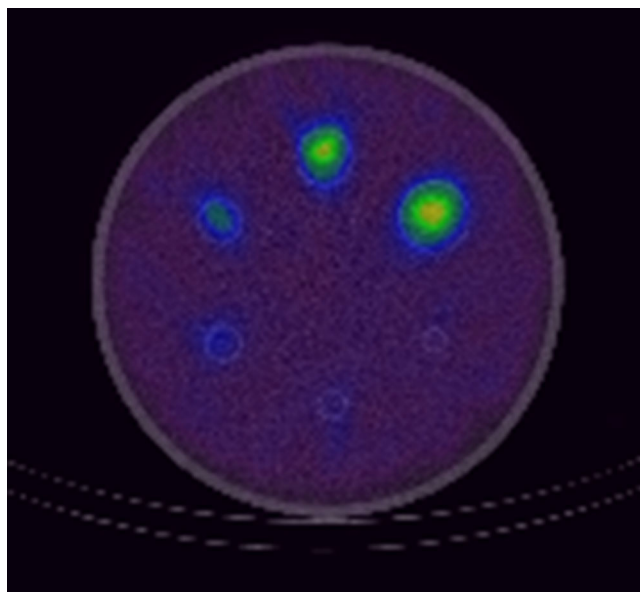


Fig. 1 Transaxial SPECT/CT fusion slice of hot spheres phantom showing the spherical inserts filled independently from phantom background.

Table 1. SPECT acquisition parameters

Parameter	Phantoms (patients) ^a
Collimator	MELP (medium energy low penetration)
Matrix/pixel size	256×256/2.4×2.4 mm
Zoom	1
Orbit/mode	Contouring/step & shoot
Scan arc/increment	360°/3°
Number of projections	120
Dwell time	30 s (15 s)
Energy windows:	Range; peak; % width
Photopeak—PP ₁₁₃	100.8–123.2 keV; 113 keV; 20 %
Photopeak—PP ₂₀₈	187.2–228.8 keV; 208 keV; 20 %
Lower scatter—LS ₁₁₃	84.00–100.2 keV; 15 %
Upper scatter—US ₁₁₃	123.2–140.0 keV; 15 %
Lower scatter—LS ₂₀₈	145.6–187.2 keV; 20 %
Upper scatter—US ₂₀₈	228.8–270.4 keV; 20 %

^aValues in parentheses describe patient settings if different from phantoms

allowed us to gather more counts to use in the scatter estimate. Furthermore, de Nijs et al. reported no significant quantitative difference between narrow and wide window widths in [20]. A summary of the SPECT and CT acquisition parameters is available in Tables 1 and 2.

Reconstruction of the data was carried out using Flash 3D, an ordered subset expectation maximization (OSEM) algorithm employing compensation for the collimator’s depth-dependent response [21]. CT attenuation and triple energy window (TEW) scatter correction [19] were also used. A range of equivalent iterations, defined as the number of updates (u) times the number of subsets (ss), was investigated, beginning with the 4u8ss used by Zeintl et al. for $^{99\text{m}}\text{Tc}$ in [22] and Beauregard et al. for ^{177}Lu in [23]. Only the number of updates was adjusted in this study, as image characteristics for a particular equivalent iteration number are known to be equivalent, provided the number of subsets is not excessively large and sufficient counts are present [24]. Each photopeak was reconstructed individually, as our software is only capable of handling one window at a time.

In addition to the default 128×128 matrix size (4.8 mm pixels), 256×256 (2.4 mm pixels) volumes were also reconstructed to minimize partial volume effects (PVEs) at sphere boundaries. The scatter projections were smoothed with a 10-mm Gaussian kernel to limit the propagation of noise via scatter correction. No post-smoothing was performed, as this is known to impose a quantitative bias by blurring activity at object edges [25, 26], and the focus of this study was quantitative accuracy rather than image quality. Reconstruction parameters are summarized in Table 3.

Table 2. CT acquisition and reconstruction parameters

Parameter	Phantoms (patients) ^a
Field of view	Same as SPECT
Collimation	2×5 mm
Pitch	1.8
Time per rotation	0.8 s
Voltage	130 kVp
Tube current	30 mAs, CARE Dose4D effective current
Reconstruction kernel	B08s, B41s (B08s, B41s)
Transverse reconstructed matrix/pixel size	512×512/0.98×0.98 mm
Slice thickness	5 mm (B08s), 3 mm (B31s, B41s)

^aValues in parentheses describe patient settings if different from phantoms

Table 3. Reconstruction parameters used for phantom experiment

Parameter	Setting
Method	Flash 3D (OSEM-based)
Corrections	Attenuation, scatter, collimator/detector response
Updates (u)/subsets (s)	4u8ss, 8u8ss, 12u8ss, 16u8ss, 20u8ss, 24u8ss, 28u8ss ^a
Photopeaks (PP _{keV})	PP ₁₁₃ , PP ₂₀₈
Transverse reconstructed matrix/pixel size	128×128/4.8×4.8 mm, 256×256/2.4×2.4 mm
Post smoothing	None (all-pass)
Scatter smoothing	10 mm

^aAn equivalent MLEM iteration is the number of updates times the number of subsets

System Calibration and Phantom Processing

In each reconstruction of the homogeneous cylinder, a 2.1-l cylindrical volume of interest (VOI) was drawn in the homogeneous background region of the phantom. A gap was left between the VOI boundary and phantom edge to minimize the influence of edge effects. From this volume, a mean count rate \hat{R} was calculated using the following formula:

$$\hat{R} = \frac{\hat{N}}{T_{\text{dur}}} \left(\frac{1}{2} \frac{e^{-(T_{\text{acq}} - T_{\text{mea}})/T_{1/2}}}{T_{1/2}} \right), \quad (1)$$

where \hat{N} is the number of counts in the VOI as allocated by the reconstruction, T_{dur} is the duration of the acquisition, T_{acq} is the acquisition start time, T_{mea} is the time of activity measurement, and $T_{1/2}$ is the half-life of ^{177}Lu . All time values were expressed in minutes. The exponential term corrects for the decay between the acquisition start and assay time, while decay occurring during the acquisition itself (−0.2 %) was neglected.

\hat{R} was then converted to the system’s estimated volumetric sensitivity \hat{S}_{VOL} via normalization by the VOI’s volume V_{VOI} in milliliters and the known measured activity concentration in the background C_{BG} in kilobecquerels per milliliter as follows:

$$\hat{S}_{\text{VOL}} = \frac{\hat{R}}{C_{\text{BG}} V_{\text{VOI}}}. \quad (2)$$

\hat{S}_{VOL} is thus expressed in units of counts per minute per milliliter per a given activity concentration and can be used to convert arbitrary regions of reconstructions from counts to kilobecquerels per milliliter. A separate \hat{S}_{VOL} was calculated for each set of reconstruction parameters.

To characterize the quantitative accuracy of each reconstruction parameter set, the corresponding calibration factor was applied to spherical VOIs drawn from each sphere in the reconstructions of the second phantom acquisition. The diameter of each VOI was set to equal the inner diameter of each (physical) sphere and centered using the CT for reference. After obtaining the count rate \hat{R}_{sph} from each sphere using Eq. 1, a corresponding recovery coefficient

$$\rho_{\text{sph}} = \frac{\left(\frac{\hat{R}_{\text{sph}}}{V_{\text{sph}} \hat{S}_{\text{VOL}}} \right)}{C_{\text{sph}}}, \quad (3)$$

was determined, where C_{sph} is the measured activity concentration in the spheres and V_{sph} is the sphere volume.

Expressed as a percentage, ρ_{sph} provides an indicator of the quantitative accuracy of a particular parameter set for a given object (spheres in this case). We also computed a noise measure $\nu = \hat{\sigma}_{\text{BG}} / \hat{\mu}_{\text{BG}}$ by normalizing the measured standard deviation of the voxels in the background VOI by their mean.

Patient Experiment

For the clinical validation, 12 SPECT/CT acquisitions from three female and six male patients, with ages ranging from 26 to 81 years (mean 62 ± 16), were included. Three patients were acquired during two consecutive therapy cycles roughly 3 months apart. Informed consent was obtained from all individual participants included in the study, which was approved by our institution's ethics commission. Each patient was receiving treatment for metastasized NETs, and the scans used for the study were undertaken as part of our clinic's protocol for PRRT therapy. The subjects were injected with 5.7–6.6 GBq (mean 6.1 ± 0.3) of [^{177}Lu]DOTATATE. The SPECT/CT acquisition was performed approximately 24 h post-injection using parameters in Tables 1 and 2.

Following the acquisition, patients were asked to void as quickly as possible, and three 1-ml urine samples were extracted for activity measurement in a calibrated well counter (MED Nuklear-Medizintechnik Dresden GmbH, Dresden). The well counter's energy window ranged from 188 to 238 keV, and the assay duration was 5 min, yielding between 25 and 150 kcts for each of our samples. Measurement was carried out several weeks after the acquisition to allow the sample to decay and avoid dead time losses. The three samples from each acquisition were then averaged and decay-corrected to T_{acq} to yield the true bladder activity concentration C_{bl} in kilobecquerels per milliliter.

Due to results presented in the next section, only PP₂₀₈ was reconstructed using 16u8ss at a 256×256 resolution for quantitative analysis. Following reconstruction, an ellipsoidal VOI was placed in the bladder with size chosen such that the maximum possible area within the bladder was covered. An example VOI is shown in Fig. 2 below, with the ellipsoid demarcated. Only acquisitions

where the bladder was large enough to accommodate a 50-ml VOI were included in this study to limit errors due to PVEs.

The total mean count rate within each VOI was then normalized by its volume and converted to kilobecquerels per milliliter using the phantom-derived calibration factor for the corresponding set of reconstruction parameters (see numerator of Eq. 3). This yielded an estimated bladder activity concentration \hat{C}_{bl} , from which the corresponding quantitative accuracy, expressed below as percentage of the true concentration, was assessed.

Results

Phantom Results

Calibration factors obtained using Eq. 2 were insensitive to all parameters except photopeak, with mean values of 1.25 ± 0.3 and 1.13 ± 0.01 cts/min/kBq for PP₁₁₃ and PP₂₀₈, respectively. Despite stable mean values, the noise level within the VOI used to determine the factors increased as a function of iteration and was higher for PP₁₁₃ than PP₂₀₈ at a given resolution and higher for the 256×256 than for the 128×128 images for a given photopeak.

Recovery coefficients for the largest sphere (16 ml) are representative and shown in Fig. 3. Each set of circle, square, triangle, and diamond markers represents a quartet of reconstructions (upper and lower photopeaks at 128×128 and 256×256 resolutions) at a particular iteration level. The iteration level increases from left to right, and a general trend of increasing recovery and noise applies regardless of energy and resolution. The reconstructions of PP₂₀₈, however, show better quantitative accuracy at a lower background variance. Relative to the $128 \times$ resolution, the $256 \times$ images yield marginally less bias at the expense of slightly greater noise for PP₂₀₈. This difference is greater for PP₁₁₃.

From the figure, it appears that the reconstruction reaches a point after which extra iterations bring little reduction in bias yet continue to amplify noise. This effect is well known in the literature [27, 25], and in this case it occurred at

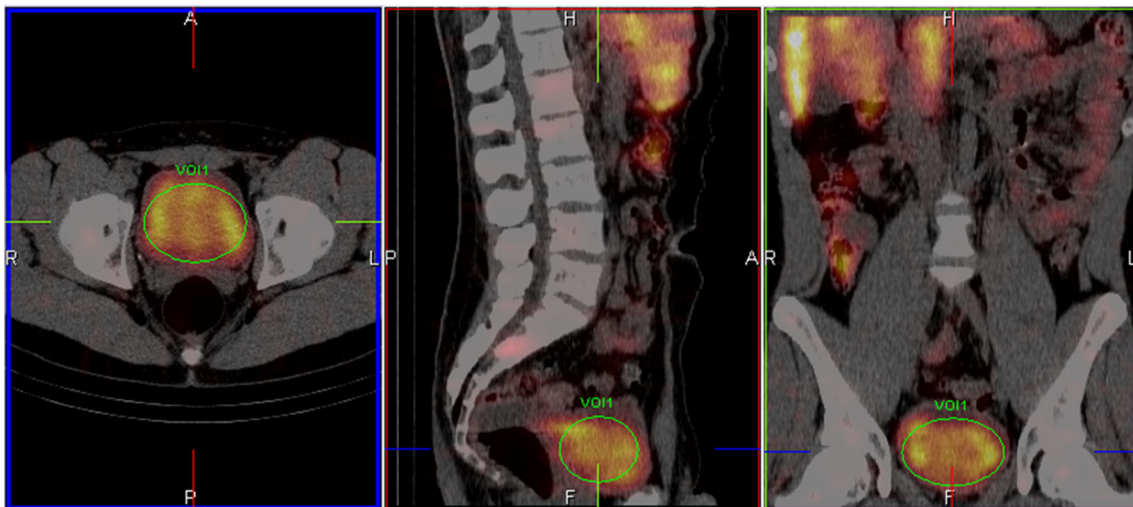


Fig. 2 Representative patient images showing ellipsoidal VOI drawn inside the bladder for quantitative analysis.

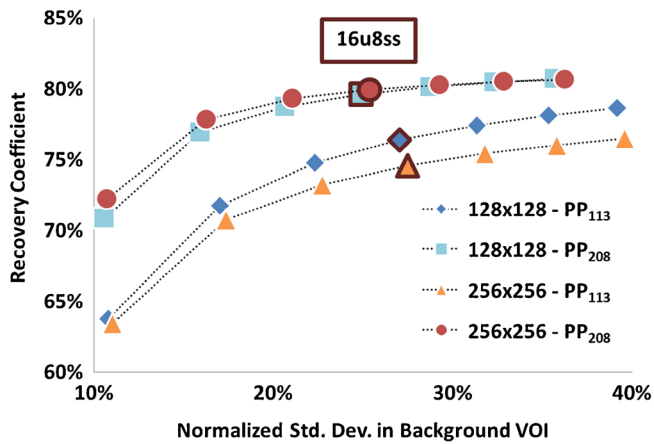


Fig. 3 Recovery coefficients versus background noise expressed as normalized standard deviation for largest sphere for various reconstruction parameter sets. For a given parameter set, iterations increase from left to right. Data obtained for 16u8ss level is highlighted with a bold border.

approximately 16u8ss. Due to this plateauing and a more favorable recovery/noise trade off, the parameter set of PP₂₀₈ at 256×256 and 16u8ss was chosen for the patient evaluation.

For the other spheres, the same trends were observed as a function of iteration number. As expected, the recovery coefficients decrease for smaller objects due to partial volume effects. Figure 4 shows the recovery coefficients for all spheres and photopeak/resolution configurations at 16u8ss. Visual evaluation of phantom images (Fig. 5) supports the quantitative results. Here, transverse slices through the 256×256 PP₂₀₈ reconstructions at each update level are shown. It can be seen that for increasing updates, the sphere boundaries become sharper, and contrast with the background increases, indicating better emission recovery.

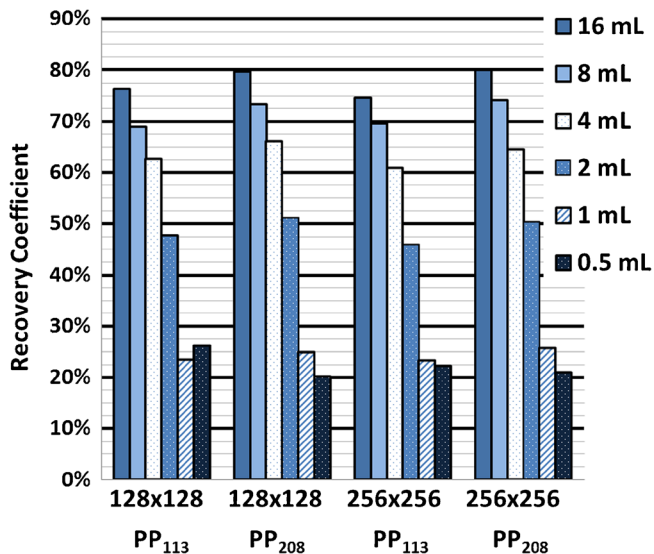


Fig. 4 Recovery coefficients for all reconstructions at 16u8ss as a function of sphere size, matrix size, and photopeak (PP).

After roughly 16u8ss, changes in contrast are difficult to discern, but noise amplification in the background is still visible.

Patient Results

The results from quantifying radioactivity concentration in the bladder are shown in Table 4. Across all acquisitions, the protocol yielded a mean recovery coefficient of 96.1±13.2 % (range, 80.6–122.4) with a 95 % confidence interval ranging from 88.6 to 103.6 %. The mean absolute error relative to the measured concentrations was 10.1±8.3 %. An underestimate was observed in most of the datasets, although four of the acquisitions exhibited overestimates. Bladder VOI sizes ranged from 56.7 to 367.4 ml, and these were not correlated with the corresponding RCs.

Figure 6 shows a Bland–Altman plot relating our estimated bladder concentrations to the measured values. A systematic underestimation of 34.3 kBq/ml is visible, but it is not statistically significant at the 5 % confidence level. Pearson’s correlation between the two methods is 0.97 ($p < 0.1$ %). Results from each of the acquisitions lie within the 95 % limits of agreement between the two methods, which we take to indicate that no outliers are present.

Discussion

Calibration and the Effect of Sphere Size, Location, and Iteration Number

Any dosimetry approach using SPECT/CT is ultimately dependent on the quantitative accuracy of the reconstructed data itself. Under our methodology, the most important physical factor driving quantitation is the value of the calibration factor, which was calculated for each reconstruction parameter set and found to be sensitive only to the choice of photopeak. The insensitivity to voxel size is expected, as the homogeneous regions used to calculate them have no edges that might be poorly represented by larger voxels. Consistency over iterations is also expected, as large objects like the cylinder background are known to converge fast relative to smaller targets [25]. However, judging from the emission probabilities for ^{177}Lu photopeaks (6.2 and 10.4 % per disintegration for PP₁₁₃ and PP₂₀₈, respectively [28]), a higher sensitivity was expected for PP₂₀₈. The fact that the converse is true can most likely be attributed to the presence of spurious counts from lead fluorescence photons and downscatter in PP₁₁₃ that was not adequately corrected for by our TEW method, as well as the higher quantum efficiency of the camera’s NaI crystal at 113 keV.

Regarding the quantification of objects, the errors of 20 % or greater are somewhat expected. The MELP collimator used here has a poor resolution compared to PET or high-resolution SPECT collimators, and even the

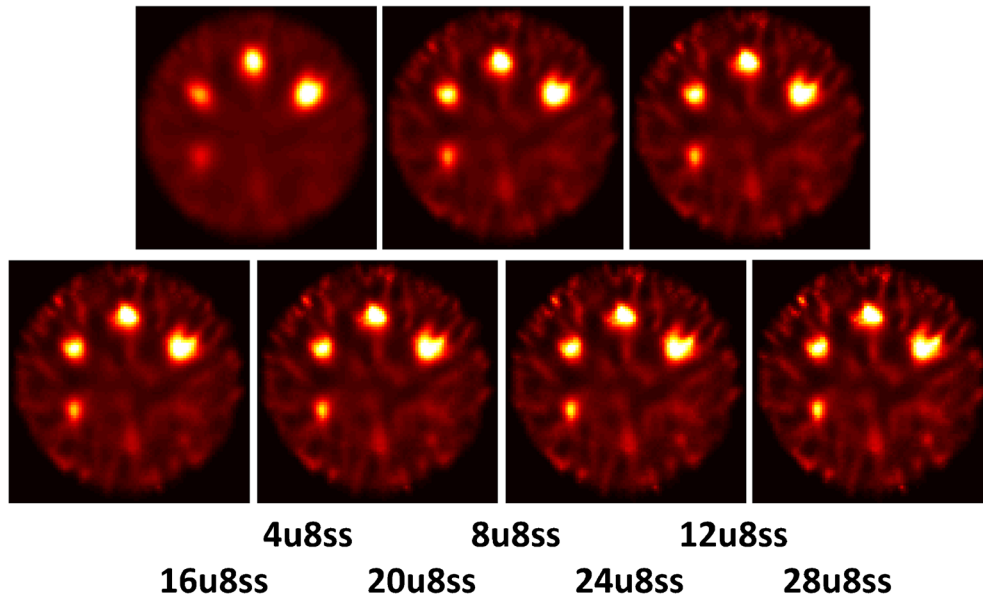


Fig. 5 Reconstructions of the sphere phantom using PP208 at 256×256 resolution at each iteration. All images are transverse slices displayed over the same window range. Note the increase in noise at higher update levels.

largest sphere is only 2.5 times wider than our system’s measured resolution, leading to unavoidable PVEs. Our CT-based VOIs are drawn at the true object edges, and the nuclear reconstruction here suffers from edge roll-off, limiting the accuracy for the largest sphere and further degrading it with decreasing sphere size. Nevertheless, our goal was to use the phantom data to select the best reconstruction settings available by comparing results across parameters, and we were able to do this despite the limits of the system.

With respect to iteration number, our results show that for small objects, a significant increase in emission recovery occurred beyond the 4u8ss recommended in [22] for $^{99\text{m}}\text{Tc}$ /LEHR acquisitions and used in [23] for the ^{177}Lu /MELP study. In [20], de Nijs et al. analyzed a range of iterations, but only for a high-resolution collimator, and noticed little difference. It is known that varying the resolution of the

collimator will affect the image’s convergence properties [29], and previous work from our group found that smaller objects require more iterations before RCs become stable [22]. As it is actually the *ratio* of collimator resolution to object size that is significant, reducing object size is analogous to decreasing collimator resolution. It is therefore reasonable that data acquired with the MELP, whose planar resolution at 10 cm we measured to be 55 % lower than the LEHR, would require more iterations for comparable quantitative accuracy.

Comparison to Results from Other Quantitative Phantom Studies

In [30], Shcherbinin et al. examined the quantitative accuracy of a small bottle containing ^{177}Lu and found a 14.2 % overshoot, albeit using very different methods involving a low-energy collimator, a different SPECT

Table 4. Results from the patient experiment

Acquisition	Recovery coefficient	VOI volume (ml)
1	80.6 %	97.0
2	100.2 %	56.7
3	119.4 %	157.9
4	102.5 %	77.6
5	95.6 %	104.4
6	122.4 %	230.15
7	88.8 %	57.74
8	81.3 %	68.3
9	90.6 %	83.3
10	91.8 %	65.7
11	88.7 %	126.4
12	91.3 %	367.4

^aAdjacent acquisitions in bold represent two studies from the same patient in consecutive therapy cycles. There were nine patients total for the 12 acquisitions, with three patients being acquired during two separate therapy cycles roughly 3 months apart

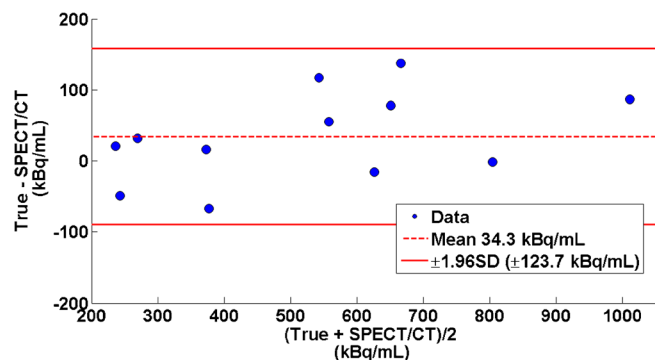


Fig. 6 Bland–Altman plot comparing estimated SPECT/CT bladder activity concentration determined *in vivo* to urine radioactivity concentration measured *in vitro*.

system, and experimental scatter correction. The performance of a commercial system very similar to ours was investigated by Beauregard et al. in [23], where activity in a phantom with two 175-ml cylindrical compartments was determined in seven experiments with varying concentration combinations. After reconstruction with 4u8ss, mean absolute errors of $7.69\pm 0.81\%$ and $9.18\pm 0.37\%$ for the two cylinders were cited, with an almost universal underestimation. The discrepancy between these values and ours at the same iteration level is presumably primarily due to the much smaller size of our objects, as even our largest 16-ml sphere will experience more PVE than the 175-ml cylinders. This is exacerbated by our selection of VOIs to match the object as shown by the CT, which is more objective but much less forgiving than the SPECT iso-contour with a 1–40 % threshold used in [23]. In that case, the authors manually adjusted the threshold for each object such that spillover activity in the background was allocated to the object of interest. This allowed them to correct for a portion of the PVEs, but the strategy is image dependent and difficult to reproduce. Comparison across reconstructions is a key component of our study, which is why we opted for the impartial CT-based VOI definition.

In addition to VOI definition, another difference in our methodology relative to Beauregard et al. is our neglect of dead time correction. Based on the Sorenson paralyzable model described in [31], the authors of [23] determined parameters for observed PP_{208} count rates in the presence of an attenuating/scattering medium that allowed them to estimate and correct for dead time loss. Using these parameters, we considered the same effect our data. These parameters were based on measurements using the same system as ours with the exception of a thicker scintillator crystal (15.8 vs. 9.5 mm). A thicker crystal will exhibit a higher quantum efficiency and deliver more pulses to the detector electronics, resulting in higher sensitivity at the risk of greater dead time losses. We measured our planar sensitivity to be 5.6 % lower than the thicker crystal cited in [23] and estimated the dead time loss for our phantom acquisitions to be 0.70 and 0.66 % for the homogeneous and sphere phantoms, respectively. When taking into account the difference in crystal thickness, we expect this value to be an overestimate and therefore negligible. Using the same method, estimated dead time in the patient studies was higher, averaging 1.42 % over all patients and projections. For some patients, dead time reached as high as 3–4 %, but only for a small number of projections during the acquisition.

The results showed superior quantitation and noise performance for PP_{208} . This is likely due to the inadequacy of the TEW method in correcting for significant downscatter in PP_{113} . In [20], de Nijs et al. also found that quantitative results from the 113-keV peak were somewhat worse than those from the 208-keV data. They reported source to background contrasts accurate to within 10 % for their optimal test case, which is more accurate than our results,

possibly due to their more advanced scatter correction method (described in [32]) and inclusion of spillover activity in the background in the VOIs being evaluated.

Although a direct comparison is not possible due to the different isotope/collimator combination, we can indirectly compare our results to the $^{99\text{m}}\text{Tc}/\text{LEHR}$ study in [22] by considering the planar resolution-to-object diameter ratio. Specifically, the RCs in the 16- and 8-ml spheres of our $^{177}\text{Lu}/\text{MELP}$ acquisition (ratios 0.39 and 0.49) should be comparable to the 4- and 2-ml spheres of the $^{99\text{m}}\text{Tc}/\text{LEHR}$ study (ratios 0.39 and 0.51). Indeed, our recovery coefficients for PP_{208} at 4u8ss and voxel size 4.8 mm are 70.9 and 61.4 % for these spheres, comparable to the 66.6 and 57.3 % values cited in the $^{99\text{m}}\text{Tc}/\text{LEHR}$ experiment at the same update level and voxel size. Residual differences may be due to differences in the orientation and contrast level of our phantom, as convergence for iterative reconstructions is object dependent [33, 34].

In Vivo Determination of Quantitative Accuracy

Despite the fact that dosimetry is a quantitative rather than diagnostic task, gains in quantitative accuracy must be weighed against increased image noise that comes with higher iterations [27, 29]. Correspondingly, data from PP_{208} with 2.4 mm pixels reconstructed with 16u8ss was chosen for our patient validation, as this parameter set yielded what we determined to be the best compromise between bias and image noise.

In patient data, this protocol yielded a mean absolute error in the bladder of roughly 10 %. Beauregard et al. cited a mean absolute error in six patients of $3.1\pm 0.47\%$ in [23], but their goal was to estimate overall activity in the body rather than concentration in a specific organ. The latter case is more difficult for SPECT due to local effects, such as poor edge resolution, that may be averaged out when an entire volume is considered. Furthermore, organ activity concentration is more closely related to the ultimate goal of 3D dosimetry. In the aforementioned $^{99\text{m}}\text{Tc}/\text{LEHR}$ quantitation study from our group, Zeintl et al. reported a mean absolute error of $6.8\pm 8.4\%$ for bladder activity concentration, which is more consistent with our results [22].

One important difference between our methodology and that of [22] is the way in which we drew our VOIs. Whereas [22] utilized an iso-contour placed around the bladder, our preliminary investigations found that even small adjustments to the iso-contour threshold caused large fluctuations in recovery coefficient—a known problem observed elsewhere [25]. To guard against these large variations, we first attempted to use a purely CT-based VOI as with the spheres but had difficulty differentiating between liquid in the bladder and the muscle tissue surrounding it on our low-dose, non-contrast-enhanced CTs. Therefore, to remain as objective and consistent as possible, we centered an ellipsoidal VOI within an activity-containing region of the

bladder. We found that, for a given image, slightly different ellipsoid sizes and placement yielded consistent results provided the ellipsoid remained within the bladder.

In addition to improved consistency and reproducibility, use of the ellipsoidal VOI also limits the influence of edge roll-off that causes the large variations in the iso-contour measurement. These edge effects can be seen in the representative patient reconstruction shown in Fig. 2. Characteristic uptake is visible in the liver, bowels, and bladder, where the transition from areas of high concentration to background at organ edges is soft and blurred. One method for mitigating this was proposed by Maus et al. in [35], where a concentric VOI a certain distance within an iso-contour was drawn. However, this method involves much subjective work in the form of setting the iso-contour threshold and manually shrinking the VOI boundary. We wanted to avoid this for reasons discussed above.

Our method of placing a VOI on the interior of the organ and avoiding the edges is more easily repeatable with less variation, yet maintains the edge-avoiding advantages of the method in [35]. A related approach was used by Sandström et al. in [18], where smaller geometric VOIs placed within organs were found to give more stable dosimetry results than attempts to include activity from the entire organ. We increased our VOI size relative to that used in [18] to mitigate the effect of noise fluctuations in the bladder seen in some of our acquisitions (also visible in Fig. 2). However, it should be noted that even if activity concentration is determined in this way, the boundary region containing activity must still be defined in order to calculate total activity for a dose estimate.

Despite encouraging results from the patient validation, our study would benefit from a larger patient collective. Furthermore, our protocol has certain limitations. Namely, due to software constraints, photon counts from Lutetium's lower energy window must be discarded. Even in the case that they could be included, our results indicate that the currently available TEW scatter correction is insufficient for correcting contamination in PP_{113} .

Another limitation of the study is that our acquisitions were carried out roughly 24 h post-injection, after which time much of the injected dose has been excreted. For dosimetry immediately following injection, activity in the patient and count rates would be much higher, and dead time correction is imperative to achieve necessary quantitative accuracy. It must also be stressed that the quantification protocol described here requires a significant amount of user interaction and additional calculations that could limit its applicability to standard clinical practice.

Conclusion

In this work, we have extended a previously published quantification protocol developed for $^{99\text{m}}\text{Tc}$ to ^{177}Lu by characterizing our commercially available SPECT/CT system's ability to quantify radioactivity concentration in small

spheres within a sphere phantom. We then validated the method's applicability to patients *in vivo* by comparing radioactivity concentration derived from quantitative SPECT/CT to urine concentration measured *in vitro*. This validation yielded mean absolute errors in the bladder of roughly 10 % or less, which is encouraging considering that quantifying activity concentration in the bladder is similar to performing the same task in the kidneys—a prerequisite for dosimetry. Our work indicates that absolute quantification of ^{177}Lu in patients for the purpose of individualized SPECT/CT PRRT dosimetry is feasible and that future work to improve physics modeling and facilitate the clinical workflow will only enhance this capability.

Acknowledgments. The authors would like thank our clinic's technologists and members of the nursing staff, each of whom greatly aided our patient data collection. We also extend our thanks to Michal Cachovan for his thoughtful discussion and technical contributions.

Conflict of Interest. James Sanders, Joachim Hornegger, and Torsten Kuwert have an ongoing research collaboration with Siemens Molecular Imaging in the field of SPECT/CT. Professor Kuwert receives honoraria from Siemens Molecular Imaging for occasional lectures pertaining to SPECT/CT research. Philipp Ritt has no conflict of interest.

Statement of Human Rights. All procedures performed in studies involving human participants were in accordance with the ethical standards of the institutional and/or national research committee and with the 1964 Helsinki declaration and its later amendments or comparable ethics standards.

References

1. Stillebroer AB, Boerman OC, Desar IME et al (2013) Phase I radioimmunotherapy study with lutetium 177-labeled anti-carbonic anhydrase IX monoclonal antibody girentuximab in patients with advanced renal cell carcinoma. *Eur Urol* 64:478–485
2. Tagawa ST, Milowsky MI, Morris M et al (2013) Phase II study of lutetium-177-labeled anti-prostate-specific membrane antigen monoclonal antibody J591 for metastatic castration-resistant prostate cancer. *Clin Cancer Res* 19:5182–5191
3. Chakraborty S, Das T, Banerjee S et al (2006) Preparation and preliminary biological evaluation of ^{177}Lu -labelled hydroxyapatite as a promising agent for radiation synovectomy of small joints. *Nucl Med Commun* 27:661–668
4. Krenning EP, Kooij PPM, Bakker WH et al (1994) Radiotherapy with a radiolabeled somatostatin analogue, [^{111}In -DTPA-D-Phe¹]-octreotide. *Ann N Y Acad Sci* 733:496–506
5. de Jong M, Bakker WH, Breeman WAP et al (1998) Pre-clinical comparison of [DTPA0] octreotide, [DTPA0, Tyr3] octreotide and [DOTA0, Tyr3] octreotide as carriers for somatostatin receptor-targeted scintigraphy and radionuclide therapy. *Int J Cancer* 75:406–411
6. Valkema R, Pauwels S, Kvols LK et al (2006) Survival and response after peptide receptor radionuclide therapy with [$^{90\text{Y}}$ -DOTA0, Tyr3]octreotide in patients with advanced gastroenteropancreatic neuroendocrine tumors. *Semin Nucl Med* 36:147–156
7. Forrer F, Valkema R, Kwekkeboom DJ et al (2007) Peptide receptor radionuclide therapy. *Best Pract Res Clin Endocrinol Metab* 21:111–129
8. Teunissen JJM, Kwekkeboom DJ, Valkema R et al (2011) Nuclear medicine techniques for the imaging and treatment of neuroendocrine tumours. *Endocr Relat Cancer* 18:S27–S51
9. Kwekkeboom DJ, Bakker WH, Kooij PP et al (2001) [^{177}Lu -DOTA0, Tyr3]octreotate: comparison with [^{111}In -DTPA0]octreotide in patients. *Eur J Nucl Med Mol Imaging* 28:1319–1325
10. de Jong M, Valkema R, Jamar F et al (2002) Somatostatin receptor-targeted radionuclide therapy of tumors: preclinical and clinical findings. *Semin Nucl Med* 32:133–140

11. Kwekkeboom DJ, de Herder WW, Kam BL et al (2008) Treatment with the radiolabeled somatostatin analog [^{177}Lu -DOTA0, Tyr3]octreotate: toxicity, efficacy, and survival. *J Clin Oncol* 28:2124–2130
12. Khan S, Krenning EP, van Essen M et al (2011) Quality of life in 265 patients with gastroenteropancreatic or bronchial neuroendocrine tumors treated with [^{177}Lu -DOTA0, Tyr3]octreotate. *J Nucl Med* 52:1361–1368
13. Watson EE, Stabin MG, Siegel JA (1993) MIRD formulation. *Med Phys* 20:511–514
14. Forrer F, Uusijärvi H, Waldherr C et al (2004) A comparison of ^{177}In -DOTATOC and ^{111}In -DOTATATE: biodistribution and dosimetry in the same patients with metastatic neuroendocrine tumours. *Eur J Nucl Med* 31(9):1257–1262
15. Ritt P, Vija H, Hornegger J, Kuwert T (2011) Absolute quantification in SPECT. *Eur J Nucl Med Mol Imaging* 38:S69–S77
16. Willowson K, Bailey DL, Baldock C (2008) Quantitative SPECT reconstruction using CT-derived corrections. *Phys Med Biol* 53:3099–3112
17. Bailey DL, Willowson KP (2014) Quantitative SPECT/CT: SPECT joins PET as a quantitative imaging modality. *Eur J Nucl Med Mol Imaging* 41:S17–S25
18. Sandström M, Garske U, Granberg D et al (2010) Individualized dosimetry in patients undergoing therapy with ^{177}Lu -DOTA-D-Phe¹-Tyr³-octreotate. *Eur J Nucl Med Mol Imaging* 37:212–225
19. Ichihara T, Ogawa K, Motomura N et al (1993) Compton scatter compensation using the triple-energy window method for single- and dual-isotope SPECT. *J Nucl Med* 34:2216–2221
20. de Nijs R, Lagerburg V, Klausen TL, Holm S (2014) Improving quantitative dosimetry in ^{177}Lu -DOTATATE SPECT by energy window-based scatter corrections. *Nucl Med Commun* 35:522–533
21. Vija AH, Hawman EG, Engdahl JC (2003) Analysis of a SPECT OSEM reconstruction method with 3D beam modeling and optional attenuation correction: phantom studies. *IEEE Nucl Sci Symp Med Imaging Conf Rec* 4:2662–2666
22. Zeintl J, Vija AH, Yahil A et al (2010) Quantitative accuracy of clinical $^{99\text{m}}\text{Tc}$ SPECT/CT using ordered-subset expectation maximization with 3-dimensional resolution recovery, attenuation, and scatter correction. *J Nucl Med* 51:921–928
23. Beauregard J-M, Hofman MS, Pereira JM et al (2011) Quantitative ^{177}Lu SPECT (QSPECT) imaging using a commercially available SPECT/CT system. *Cancer Imaging* 11:56–66
24. Hudson HM, Larkin RS (1994) Accelerated image reconstruction using ordered subsets of projection data. *IEEE Trans Med Imaging* 13:601–609
25. Dewaraja YK, Frey EC, Sgouros G et al (2012) MIRD Pamphlet no. 23: quantitative SPECT for patient-specific 3-dimensional dosimetry in internal radionuclide therapy. *J Nucl Med* 53:1310–1325
26. Chun SY, Fessler JA, Dewaraja YK (2013) Post-reconstruction non-local means filtering methods using CT side information for quantitative SPECT. *Phys Med Biol* 58:6225–6240
27. Tsui BMW, Zhao XD, Frey EC (1991) Comparison between ML-EM and WLS-CG algorithms for SPECT image reconstruction. *IEEE Trans Nucl Sci* 38:1766–1772
28. Schötzig U, Schrader H, Schönfeld E et al (2001) Standardisation and decay data of ^{177}Lu and ^{188}Re . *Appl Radiat Isot* 55:89–96
29. Hutton BF, Hudson HM, Beekman FJ (1997) A clinical perspective of accelerated statistical reconstruction. *Eur J Nucl Med Mol Imaging* 24:797–808
30. Shcherbinin S, Piwowska-Bilska H, Celler A, Birkenfeld B (2012) Quantitative SPECT/CT reconstruction for ^{177}Lu and $^{177}\text{Lu}/^{90}\text{Y}$ targeted radionuclide therapies. *Phys Med Biol* 57:5733–5747
31. Sorenson JA (1975) Deadtime characteristics of Anger cameras. *J Nucl Med* 16:284–288
32. Frey EC, Tsui BMW (1996) A new method for modeling the spatially-variant, object-dependent scatter response function in SPECT. *IEEE Nucl Sci Symp Med Imaging Conf Rec* 2:1082–1086
33. Fessler JA, Rogers WL (1996) Spatial resolution properties of penalized-likelihood image reconstruction: space-invariant tomographs. *IEEE Trans Image Proc* 5:1346–1358
34. Liow JS, Strother SC (1993) The convergence of object dependent resolution in maximum likelihood based tomographic image reconstruction. *Phys Med Biol* 38:55–70
35. Maus J, Hofheinz F, Schramm G et al (2014) Evaluation of PET quantification accuracy in vivo. *Nuklearmedizin* 53:67–77